ELSEVIER

Journal of Alloys and Compounds 436 (2007) 1–8

Journal of ALLOYS AND COMPOUNDS

www.elsevier.com/locate/jallcom

Magnetic ordering in the $HfFe_6Ge_6$-type $TbFe_6Sn_4Ge_2$ compound

Laura K. Perry [a], D.H. Ryan [a,*], G. Venturini [b], B. Malaman [b]

[a] *Centre for the Physics of Materials and Physics Department, McGill University, Montréal, Que. H3A 2T8, Canada*
[b] *Laboratoire de Chimie du Solide Minéral, Université Henri Poincaré-Nancy I, associé au CNRS (UMR 7555), BP 239, 54506 Vandoeuvre les Nancy Cedex, France*

Received 18 May 2006; received in revised form 26 June 2006; accepted 27 June 2006
Available online 7 August 2006

Abstract

We have determined the magnetic structures of the Tb and Fe sublattices in $TbFe_6Sn_4Ge_2$ by combining powder neutron diffraction with ^{57}Fe and ^{119}Sn Mössbauer spectroscopy. $TbFe_6Sn_4Ge_2$ adopts the hexagonal $HfFe_6Ge_6$-type ($P6/mmm$) crystal structure. The Fe sublattice orders antiferromagnetically below $T_N = 518(3)$ K, with the moments parallel to c. At $T_t = 42(1)$ K, the Tb sublattice orders helimagnetically, with a propagation vector $Q = (0, 0, 0.0963)$ r.l.u. (at 2 K). This imposes helimagnetic order (with an identical propagation vector) on the Fe sublattice, indicating that the two sublattices are coupled for $T < T_t$. The canting angle of the Fe moments from the c-axis in the helimagnetic structure is 10(1)°.

Keywords: Terbium; Iron; Tin; Germanium; Antiferromagnetic; Helimagnetic order; ^{119}Sn Mössbauer; Neutron scattering; ^{57}Fe Mössbauer

1. Introduction

The RFe_6X_6 family of compounds (R = Y, Gd–Lu; X = Sn, Ge) displays magnetic behaviour which is unique among the intermetallic compounds: the Fe and rare earth sublattices order independently [1–5]. These compounds crystallize in orthorhombic *Immm* or *Cmcm* structures, which consist of a complicated stacking of $HfFe_6Ge_6$-type and $ScFe_6Ga_6$-type slabs. In the $ErFe_6Sn_{6-x}Ga_x$ series, a transition from the orthorhombic to the hexagonal $HfFe_6Ge_6$-type structure was observed for $0.25 < x < 2.5$ [6]. This suggests that the substitution of Sn by the smaller Ga (or Ge) atoms leads to the stabilization of the hexagonal structure. The $HfFe_6Ge_6$-type crystal structure is much simpler than the orthorhombic structures of ternary RFe_6Sn_6 compounds, and so provides a simpler environment in which to study the interactions between the rare earth and Fe sublattices.

A recent investigation of $RFe_6Sn_4Ge_2$ has confirmed the stabilization of the hexagonal structure, driven by the partial replacement of Sn by Ge [7]. Here we use powder neutron diffraction combined with ^{57}Fe and ^{119}Sn Mössbauer spectroscopy to study the magnetic structure of $TbFe_6Sn_4Ge_2$, and show that the Fe and rare earth sublattices indeed order at different temperatures, but are coupled in such a way that the ordering of Tb at T_t changes the magnetic properties of the Fe sublattice. This behaviour is unique within the RFe_6X_6 (X = Sn, Ge) family of compounds.

2. Experimental methods

The $TbFe_6Sn_4Ge_2$ sample was prepared by alloying stoichiometric amounts of the elements (99.99% pure) in an induction furnace. The resulting ingot was annealed at 1123 K for 1 week, then it was ground, compacted and annealed at the same temperature for another week. The composition of the $TbFe_6Sn_4Ge_2$ sample was verified by conventional X-ray powder analysis (Guinier Cu Kα). The main impurity lines were Sn (6%) and Tb_2O_3 (2%). The neutron diffraction sample contains small amounts of free iron (2%) which was removed magnetically for the Mössbauer study. The neutron diffraction patterns were recorded on the D1B diffractometer at the Institut Laue Langevin (Grenoble) with a wavelength $\lambda = 2.520$ Å. Three long duration patterns were taken at 300, 100 and 2 K. Short duration patterns in the 2–100 K temperature range enabled tracking of the intensity of magnetic satellites with temperature, yielding the rare earth ordering temperature, T_t. All refinements of the neutron and X-ray diffraction patterns were carried out using the FULLPROF/WinPlotr package [8].

^{57}Fe and ^{119}Sn transmission Mössbauer spectra were collected on a constant acceleration spectrometer, which was calibrated with α-Fe and a ^{57}Co source. For ^{57}Fe Mössbauer spectroscopy, a 50 mCi Rh ^{57}Co source was used, and for ^{119}Sn, the source was 10 mCi ^{119m}Sn $CaSnO_3$.

* Corresponding author. Tel.: +1 514 398 6534; fax: +1 514 398 8434.
E-mail address: dhryan@physics.mcgill.ca (D.H. Ryan).

0925-8388/$ – see front matter © 2006 Elsevier B.V. All rights reserved.
doi:10.1016/j.jallcom.2006.06.099

The sample was kept in a vibration-isolated closed-cycle refrigerator, and the temperature was varied from 12 to 300 K. For the 5 K ^{119}Sn spectrum, the sample was placed in a helium flow cryostat. All of the spectra were fitted with a conventional non-linear least-squares minimization routine, which uses a sum of Lorentzian lineshapes. For the ^{57}Fe spectra, the line positions were calculated as a first order perturbation because the hyperfine field at the Fe site far exceeds any quadrupole splitting. In contrast, the magnitude of the quadrupole splitting is very close to that of the hyperfine field for one of the ^{119}Sn subspectra, and a full Hamiltonian solution was required to fit the spectra [9].

3. Results and discussion

3.1. Crystal structure

The crystal structure is of the $HfFe_6Ge_6$-type (space group $P6/mmm$, no. 191). Fig. 1 shows the hexagonal structure of $TbFe_6Sn_4Ge_2$, which has one Tb (Tb-1a), one Fe (Fe-6i), and three Sn sites (Sn-2c, Sn-2d and Sn-2e). This is a simpler structure than that of $TbFe_6Sn_6$ (orthorhombic, $Cmcm$), characterized by one Tb, three Fe and five Sn sites [10].

Preliminary studies showed that Ge substitutes mainly at the 2c position [7]. In the inital refinement of the 300 K neutron diffraction pattern (shown in Fig. 2), we therefore assumed that the 2c site was fully occupied by Ge, while the two remaining Sn sites were fully occupied by Sn. Refining the occupation factors, we found an increase for Sn-2d and a decrease for Sn-2c and Sn-2e. Owing to the relative Fermi lengths of Ge and Sn, this indicates that Sn-2d is partially occupied by Ge 10(4)%, (see Table 1), and Sn-2c is partially occupied by Sn 17(4)%, (see Table 1). The decrease in the Sn-2e occupation factor, however, cannot be accounted for by Ge–Sn mixing. Therefore, in the final refinement, the Sn occupation at Sn-2e was fixed to 100%. At low temperature, the Sn occupations were fixed to those determined at 300 K. Table 1 summarizes the refined parameters from neutron diffraction data at 300, 100 and 2 K.

In contrast to $TbFe_6Sn_6$, we observe a shift in the position of the Fe atom on the c-axis ($z_{Fe} = 0.2342(8)$), which results from Ge doping. This indicates that the Fe atom moves towards the site on which the substitution occurs, Sn-2c, as the site volume decreases when substituted with the smaller Ge atom. As a result, the corresponding Fe–Ge(Sn-2c) distance (2.538 Å) is significantly smaller than the Fe–Sn distances (2.762 and 2.802 Å for Sn-2d and Sn-2e respectively).

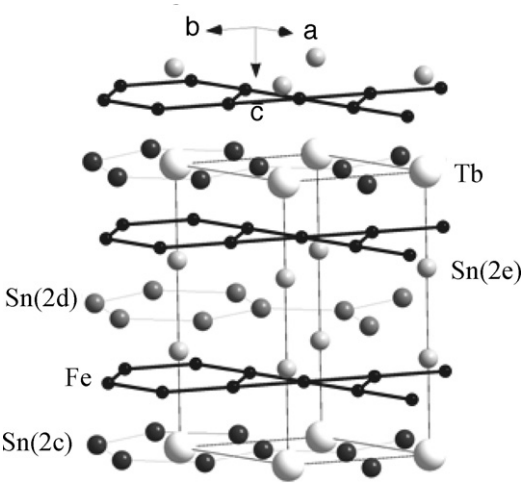

Fig. 1. $HfFe_6Ge_6$-type crystal structure of $TbFe_6Sn_4Ge_2$. From neutron diffraction, the Sn occupation at Sn-2c is 17% (83% Ge), Sn-2d has a 90% Sn occupation, and Sn-2e is fully occupied by Sn.

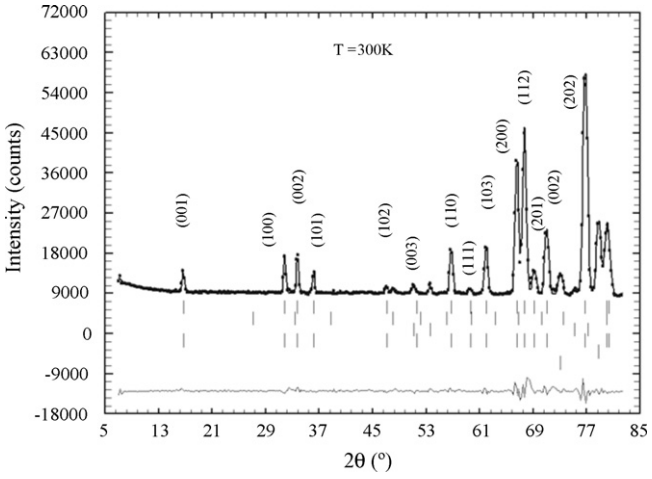

Fig. 2. Neutron diffraction pattern of $TbFe_6Sn_4Ge_2$ at 300 K. All of the lines are indexed, and the main impurities are Sn (6%) and Tb_2O_3 (2%). From top to bottom, the Bragg markers correspond to: (1) nuclear $TbFe_6Sn_4Ge_2$, (2) Tb_2O_3, (3) Sn, (4) antiferromagnetic $TbFe_6Sn_4Ge_2$ and (5) the vanadium sample holder.

3.2. Magnetic structure for $T_N > T > T_t$

The neutron diffraction patterns at 300 and 100 K show lines which are characteristic of the hexagonal $HfFe_6Ge_6$-type ($P6/mmm$) crystal structure (Fig. 2). Magnetometry measurements showed that the Fe sublattice orders antiferromagnetically below $T_N = 518(3)$ K [7] and therefore all diffraction patterns have been recorded in the ordered magnetic state. Comparison between the observed patterns and those calculated with only nuclear contributions, indicates minimal magnetic intensity contributions to ($h\,k\,l$) lines with odd l. As the iron atoms are located near $z = 1/4$ and 3/4, this behaviour is typical of a magnetic arrangement of ferromagnetic Fe planes alternating up

Table 1
Summary of the refined parameters for $TbFe_6Sn_4Ge_2$ from neutron scattering

	300 K	100 K	2 K
a (Å)	5.2903(7)	5.2758(7)	5.2731(5)
c (Å)	8.658(1)	8.640(1)	8.636(1)
z_{Fe}	0.2342(8)	0.2348(8)	0.2358(7)
z_{Sn} (Sn-2e)	0.341(1)	0.342(1)	0.339(1)
%Sn (Sn-2c)	17(4)	*	*
%Sn (Sn-2d)	90(4)	*	*
%Sn (Sn-2e)	100	*	*
μ_{Fe}AF (μ_B)	2.02(5)	2.32(4)	2.34(5)
μ_{Fe}Heli (μ_B)	–	–	0.40(4)
μ_{Tb}Heli (μ_B)	–	–	6.84(9)
q_z	–	–	0.0963(4)
ϕ_{Fe}	–	–	230(7)°

Note: The low temperature Sn occupation factors (%Sn), were constrained to the values determined at 300 K.

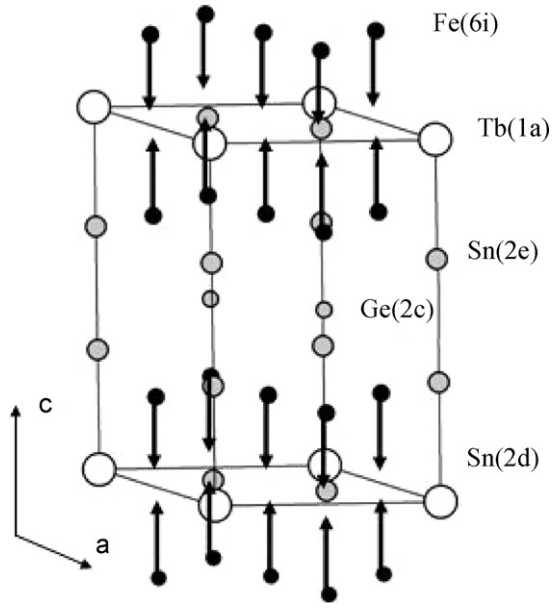

Fig. 3. Unit cell of the magnetic structure of $TbFe_6Sn_4Ge_2$ for $T_N > T > T_t$.

and down along the [0 0 1] direction. The absence of magnetic contributions to the (0 0 l) lines indicates that the Fe moments are directed along the *c*-axis. The structure therefore consists of ferromagnetic (0 0 1) Fe planes, antiferromagnetically coupled and stacked along the *c*-axis as Fe(↑)Fe(↓)Fe(↑)Fe(↓) (Fig. 3), a stacking typical of the RFe_6Sn_6 compounds (R = Sc, Ti, Zr, Nb, Hf, lanthanides; X = Sn, Ge). Finally, the Fe magnetic moment (μ_{Fe}) is close to that measured in the RFe_6Sn_6 (R = Sc, Y, Zr, Er, Tm, Lu) ternary stannides [11,18], summarized in Table 2.

3.2.1. Mössbauer spectroscopy

The ^{57}Fe Mössbauer spectrum at 300 K shown in Fig. 4 (left) was fitted with a single sextet corresponding to the Fe-6i site. Table 3 lists the ^{57}Fe Mössbauer parameters at 300 K, and compares them with those of other RFe_6X_6 compounds (R = Er, Yb; X = Sn, Ge). Fig. 4 (right) shows the ^{119}Sn Mössbauer spectrum at 300 K. The spectrum shows three distinct subspectra, which correspond to the three Sn sites of the crystal structure. The area ratio of the three Sn sites at 300 K is 7(2):44(1):49(1) for Sn-2c, Sn-d and Sn-2e, respectively (other ^{119}Sn Mössbauer parameters are shown in Table 3). Assuming that the Sn-2e site is fully occupied by Sn, the spectral areas yield Sn occupations of 15(4), 91(2) and 100% for Sn-2c, Sn-2d and Sn-2e, in full agreement with the site occupations determined through neutron scattering (%Sn in Table 1).

Previous studies of $TbMn_6Sn_{5.46}In_{0.54}$, which adopts the same $HfFe_6Ge_6$-type crystal structure as $TbFe_6Sn_4Ge_2$, showed that the principal axis of the electric field gradient, V_{zz}, was parallel to the *c*-axis for all three Sn sites [21,22]. Since the structures are the same and the quadrupole splittings are comparable, we will assume here that V_{zz} for the three Sn sites in $TbFe_6Sn_4Ge_2$ is also parallel to *c*. Two of the three Sn sites (2*c* and 2*d*) lie between two antiferromagnetically coupled Fe planes and so there is no transferred hyperfine field, however the Sn-2e site is located almost within an Fe plane and experiences a significant transferred field from the ring of six parallel Fe moments. If we define θ, as the angle between B_{hf} and V_{zz}, then it is 0° for the

Table 3
^{57}Fe and ^{119}Sn Mössbauer parameters for $TbFe_6Sn_4Ge_2$, as well as for other RFe_6X_6 (X = Sn, Ge) compounds, at 300 K

Compound	Site	B_{hf} (T)	Δ (mm/s)	Reference
^{57}Fe				
$TbFe_6Sn_4Ge_2$	Fe-6i	18.49(2)	0.266(5)	*
$ErFe_6Sn_6$	Average	20.1(1)	–	[18]
$YbFe_6Ge_6$	Fe-6i	14.8(1)	−0.26(3)	[16]
^{119}Sn				
$ErFe_6Sn_6$	64(2)%	0	–	[18]
$ErFe_6Sn_6$	36(2)%	22.2(1)	–	[16]
$TbFe_6Sn_4Ge_2$	Sn-2c	0	0	*
$TbFe_6Sn_4Ge_2$	Sn-2d	0	1.42(1)	*
$TbFe_6Sn_4Ge_2$	Sn-2e	18.53(2)	0.4(3)	*
$HoFe_6Sn_6$	63(1)%	0	–	[3]
$HoFe_6Sn_6$	37(1)%	22.3(1)	–	[3]

Due to the complicated orthorhombic structures, the sites in the Er and Ho compounds were averaged to determine B_{hf}. Note that in the Sn compounds, 2/3 of the Sn sites have zero B_{hf} as a result of cancellations due to the antiferromagentic structure.

Table 2
Iron magnetic moments in RFe_6X_6 (X = Sn, Ge), measured by neutron diffraction

R	Stannides			Germanides		
	Type	μ_{Fe} (μ_B)	Reference	Type	μ_{Fe} (μ_B)	Reference
Sc	$HfFe_6Ge_6$	2.35(5)	[11]	$HfFe_6Ge_6$	1.52(4)	[12]
Ti	–	–	–	$HfFe_6Ge_6$	1.68(6)	[12]
Y	$HoFe_6Sn_6$	2.14(6)	[13]	$TbFe_6Sn_6$	1.88(6)	[14]
Zr	$HfFe_6Ge_6$	2.31(5)	[11]	$HfFe_6Ge_6$	1.96(4)	[12]
Nb	–	–	–	$HfFe_6Ge_6$	2.05(5)	[12]
Tb	$TbFe_6Sn_6$	–	–	$TbFe_6Sn_6$	2.29(6)	[15]
Dy	$DyFe_6Sn_6$	–	–	$TbFe_6Sn_6$	2.20(22)	[16]
Ho	$HoFe_6Sn_6$	2.31(5)	[3]	$TbFe_6Sn_6$	1.80(7)	[17]
Er	$ErFe_6Sn_6$	2.4(6)	[18]	$HoFe_6Sn_6$	2.0(2)	[15]
Tm	$HfFe_6Ge_6$	2.40(4)	[11]	$ErFe_6Sn_6$	–	–
Yb	–	–	–	$HfFe_6Ge_6$	1.72(5)*	[19]
Lu	$HfFe_6Ge_6$	2.40(4)	[11]	$HfFe_6Ge_6$	1.45(3)*	[20]
Hf	–	–	–	$HfFe_6Ge_6$	1.9(1)	[20]

All measurements (except those marked) * were made for $T \ll T_N$, and for compounds with paramagnetic rare earths, the data were taken below T_t (the ordering temperature of the rare earth). Exceptions are: $LuFe_6Ge_6$, $T = 293$ K, and $YbFe_6Ge_6$, $T = 1.5$ K, above which the Yb sublattice shows no long range order.

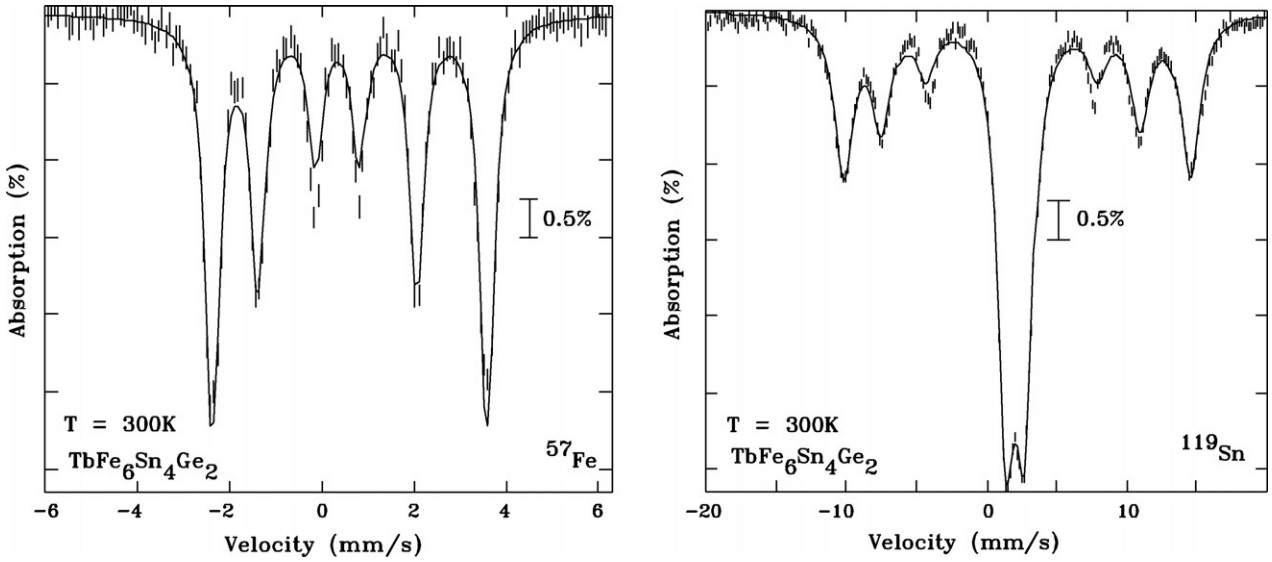

Fig. 4. Left: ^{57}Fe and right: ^{119}Sn Mössbauer spectra of $TbFe_6Sn_4Ge_2$ at 300 K.

Sn-2e site because the Fe moments contributing to B_{hf} are all parallel to c.

3.3. Magnetic structure for $T < T_t$

3.3.1. ^{119}Sn Mössbauer spectroscopy

Fig. 5 (left) shows the ^{119}Sn Mössbauer spectra of $TbFe_6Sn_4Ge_2$, from 300 to 5 K. The spectral areas were constrained to those determined at 300 K. Note that at low temperature, a fourth component appears in the spectra, which corresponds to a Sn impurity (Debye temperature 131(12) K and isomer shift $\delta = 2.7(1)$ mm/s). Hyperfine parameters are shown in Table 4 for 50 and 5 K.

The temperature dependence of the hyperfine field is shown in Fig. 5 (right). Below 40 K, a small hyperfine field of ~0.3 T develops at the Sn-2d site, which increases to 1.02(5) T by 5 K. The temperature dependence of this field gives a transition temperature of $T_t = 38(3)$ K, well above the previously reported $T_t = 25.4(5)$ K [7]. Since the magnitude of the quadrupole splitting is very close to that of the hyperfine field at Sn-2d (Table 4), a full Hamiltonian solution was required to fit the ^{119}Sn spectra. The appearance of a small B_{hf} at Sn-2d for temperatures below $T_t = 38(3)$ K marks an event which is most likely due to the ordering of the Tb sublattice. A slight change in B_{hf} at Sn-2e is the only other consequence of this ordering, and there are no changes in quadrupole splitting. The angle θ between V_{zz} and B_{hf} (V_{zz} was previously assumed to be parallel to c), is found to be 90° for Sn-2d. This indicates that the new hyperfine field at the Sn-2d site lies in the *ab*-plane, and is thus perpendicular to the Fe order which existed for $T_N > T > T_t$. As the first Tb neighbour is much further from Sn-2d (5.298 Å) than the six nearest Fe neighbours (2.726 Å), the new field at Sn-2d is more likely due to a modification of the Fe sublattice in response to the ordering of Tb, rather than a direct consequence of the Tb ordering. This provides the first evidence, in this family of compounds, for a non-negligible interaction between the rare earth and transition metal sublattices.

Table 4
^{119}Sn Mössbauer parameters for $TbFe_6Sn_4Ge_2$ at 50 and 5 K

Site	B_{hf} (T)	Δ (mm/s)	θ(°)
$T = 50$ K ($T > T_t$)			
Sn-2c	0	0	–
Sn-2d	0	1.57(3)	–
Sn-2e	20.34(2)	0.45(2)	0
$T = 5$ K ($T > T_t$)			
Sn-2c	0	0	–
Sn-2d	1.02(5)	1.43(9)	90
Sn-2e	20.20(2)	0.44(3)	0

The angle θ is that between B_{hf} and V_{zz}, the principal axis of the electric field gradient.

3.3.2. Neutron scattering

The 2 K neutron diffraction pattern in Fig. 6 is similar to the high temperature patterns, but with several additional lines. The symmetrical location of the lines around the (0 0 1), (1 0 1) and (1 0 2) nuclear peaks suggests they are satellites of these lines with propagation vector $Q = (0, 0, q_z)$. This assumption has been confirmed using a least squares fitting software, giving $q_z = 0.0963(2)$ r.l.u. (reciprocal lattice units). q_z is nearly constant at $q_z = 0.0963(2)$ r.l.u. up to 15 K, and then increases to $q_z = 0.122(3)$ r.l.u. by T_t, as shown in Fig. 7 (left). The temperature dependence of the $(0\,0\,1)^-$ satellite shown in Fig. 7 (right) provides an estimate of the transition temperature, measured here at $T_t = 42(1)$ K, below which the Tb sublattice is helimagnetically ordered. This transition temperature is significantly higher than that deduced from magnetometry measurements [7], but is consistent with the value of 38(3) K derived from ^{119}Sn Mössbauer spectroscopy.

For all other RFe_6Sn_6 alloys, the changes in the low temperature neutron diffraction patterns could be accounted for by considering only the ordering of the rare earth moment. In the current study, such a refinement of the 2 K pattern fails, resulting in a residual factor of $R_H = 22\%$. Furthermore, including a contribution from the Tb sublattice alone does not account for

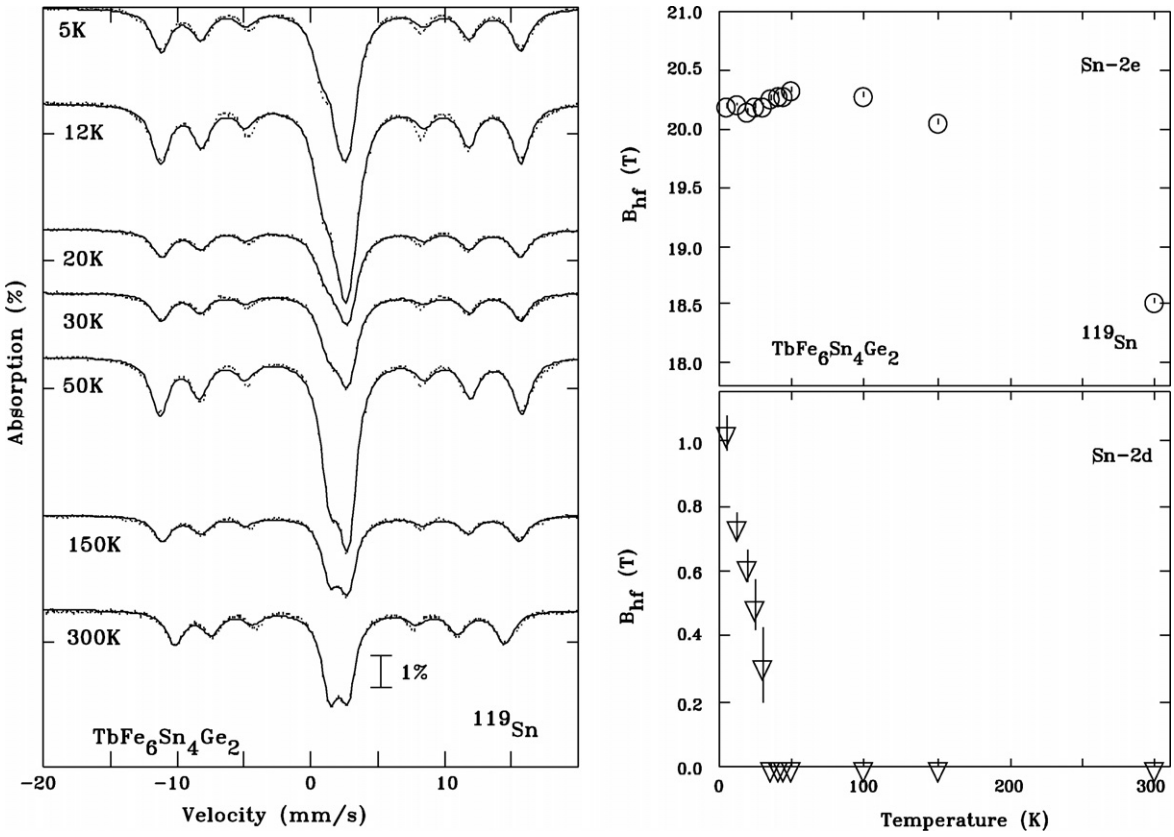

Fig. 5. Left: ^{119}Sn Mössbauer spectra, from 300 to 5 K. Right: hyperfine fields at the Sn(2e) and Sn(2d) sites in $TbFe_6Sn_4Ge_2$. The transferred hyperfine field at Sn(2e) persists over the whole studied temperature range (decreasing only slightly at T_t), and that at Sn(2d) exists only for $T < T_t$.

the asymmetric intensities of the $(0\,0\,1)^-$ and $(0\,0\,1)^+$ satellites. From Mössbauer spectroscopy, we already anticipate a modification of the Fe sublattice in response to the Tb order. Since there are no notable changes in the intensities of the lines on cooling through T_t, the effect on the Fe order must be small. If a helimagnetic contribution from the Fe sublattice is considered, the propagation vector must be the same as that of the Tb sublattice, because no new satellites appear for $T < T_t$ which would indicate the formation of a second incommensurate magnetic structure. In the final refinement we thus included helimagnetic contributions from both the Tb and the Fe sublattices. $TbFe_6Sn_4Ge_2$ is the only compound of the RFe_6Sn_6 series for which this co-dependence exists.

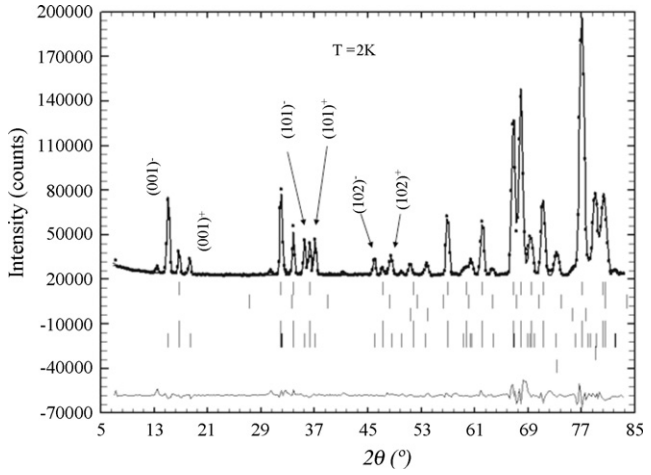

Fig. 6. Neutron diffraction pattern of $TbFe_6Sn_4Ge_2$ at 2 K. From the $(0\,0\,1)^+$ and $(0\,0\,1)^-$ satellites, we determine that the structure is helimagnetic, with a propagation vector $Q = (0, 0, 0.0963(2))$ (at 2 K). From top to bottom, the Bragg markers correspond to (1) nuclear $TbFe_6Sn_4Ge_2$, (2) Tb_2O_3, (3) Sn, (4) antiferromagnetic $TbFe_6Sn_4Ge_2$, (5) helimagnetic $TbFe_6Sn_4Ge_2$ and (6) the vanadium sample holder.

Refining the Tb moment fixes the origin of the phase angle ($\phi_{Tb} = 0$) and the Fe helimagnetic component, for which the phase angles ϕ_{Fe} and $-\phi_{Fe}$ are attributed to the Fe planes lying at $z = 1/4$ and 3/4, respectively. The tilt angle θ between the normal of the helical plane and the c-axis was constrained to be the same for both sublattices and is close to 0°. The helical components therefore rotate in the $(0\,0\,1)$ plane. This suggests an easy plane anisotropy for the Tb sublattice, in contrast to the easy axis anisotropy observed in $TbMn_6Sn_6$ [23]. The results of the refinements are given in Table 1, and a representation of the magnetic structure for $T < T_t$ is shown in Fig. 8. The magnetic structure for $T < T_t$ is constructed as a combination of the original antiferromagnetic order of the Fe sublattice (with moment μ_{Fe}(AF), Table 1), along with two helimagnetic contributions (one from Tb and one from Fe) with identical propagation vectors (Fig. 8). The canting angle of the Fe moments can be estimated through

$$\theta = \arctan\left(\frac{\mu_{Fe}(AF)}{\mu_{Fe}(Heli)}\right) = \arctan\left(\frac{2.34(5)}{0.40(4)}\right) = 10(1)^\circ \quad (1)$$

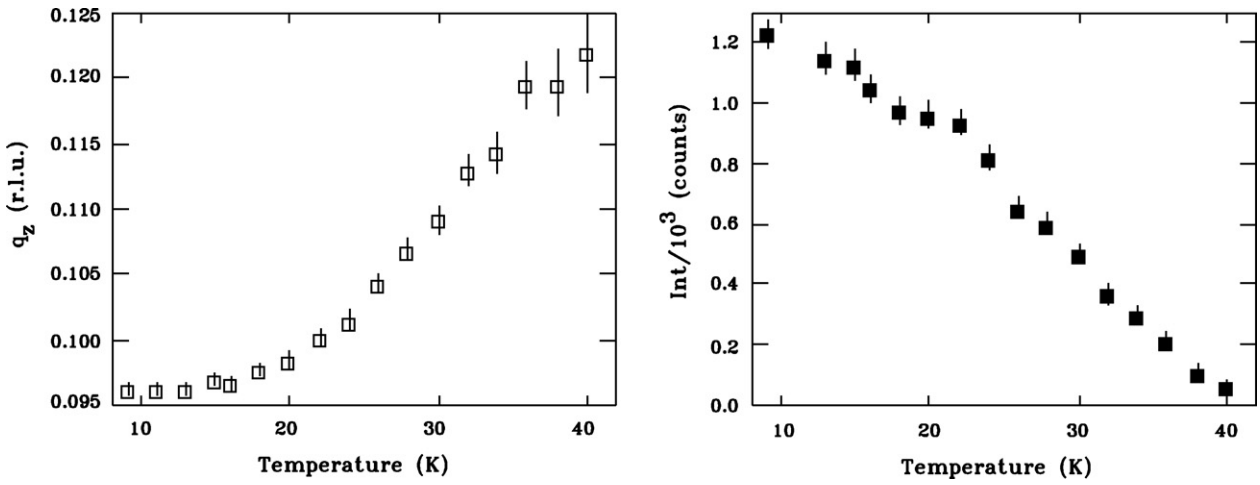

Fig. 7. Left: temperature dependence of the z component of the propagation vector, q_z. Right: intensity of the $(0\,0\,1)^-$ satellite as a function of temperature. From this dependence we get a transition temperature of $T_t = 42(1)$ K, consistent with that measured using ^{119}Sn Mössbauer spectroscopy.

where μ_{Fe}(AF) is the antiferromagnetic Fe moment, and μ_{Fe}(Heli) is the helimagnetic Fe moment. Both magnitudes are measured at 2 K.

It should be noted that the angles between the helimagnetic contribution from the Fe moments belonging to adjacent layers differ. Within the Fe–(Ge,Tb)–Fe slab, this angle is 117°, and within the Fe–Sn–Sn–Sn–Fe slab, it is 82°. The larger angle for Fe–(Ge,Tb)–Fe may indicate that the antiferromagnetic interactions within the slab are stronger. This is supported by the corresponding interlayer distances, which are shorter for Fe–(Ge,Tb)–Fe (4.055 Å) than for Fe–Sn–Sn–Sn–Fe (4.602 Å). The angle between the Tb moment and the surrounding helimagnetic Fe components is close to 121°, thus accounting for the antiferromagnetic interaction between Tb and the 3d moments.

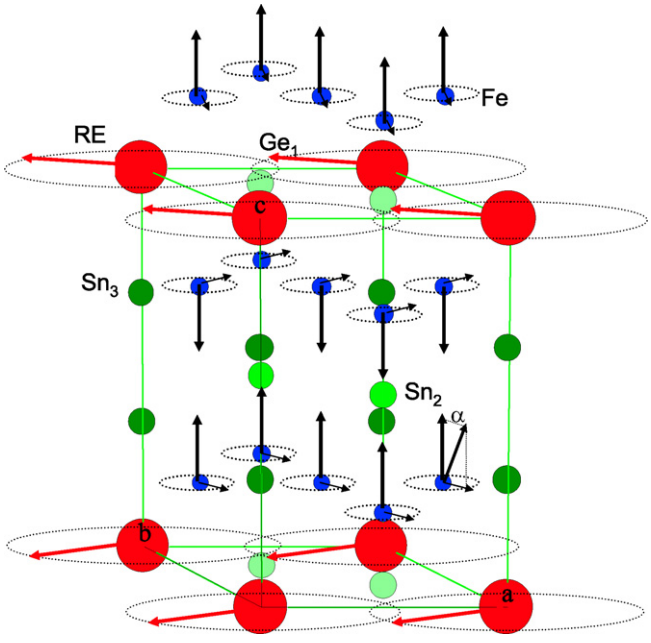

Fig. 8. Unit cell of the magnetic structure of $TbFe_6Sn_4Ge_2$ for $T < T_t$. The canting of the Fe moments by 11(3)° above and below the Sn-2d site is such that the transferred hyperfine field at Sn-2d is non-zero.

3.3.3. ^{57}Fe Mössbauer spectroscopy

Fig. 9 shows the temperature dependence of the ^{57}Fe Mössbauer spectra (left), from 300 to 12 K. In the high-temperature structure ($T > T_t$), the Fe moments are parallel to the c-axis. Neutron scattering showed that the moments tilt away from the c-axis by 10(1)° on cooling through T_t. In order to determine the change in moment direction through Mössbauer spectroscopy, it is necessary first to define a reference frame. In a powdered sample, the electric field gradient (quadrupole splitting) can be chosen as a reference frame. The expression for the quadrupole splitting for a first-order perturbation (used to fit the ^{57}Fe spectra) is given by

$$\Delta = \frac{eQV_{zz}}{4}(3\cos^2\theta - 1) \quad (\eta = 0) \tag{2}$$

where θ is defined as the angle between the hyperfine field and the principal axis of the electric field gradient tensor, V_{zz}, and η is the asymmetry parameter.

There is no significant anomaly in the ^{57}Fe hyperfine field at the T_t transition (Fig. 9, bottom right), consistent with the transition affecting only the direction of the magnetic moments. However T_t is marked by a clear change in quadrupole splitting below 50 K (Fig. 9, top right), yielding $T_t = 43(4)$ K, consistent with the previous two measurements reported here. The canting angle can be determined from this change in quadrupole splitting, but the analysis depends on the assumed direction of V_{zz} within the crystal axis system. The high symmetry of the sites in the hexagonal $HfFe_6Ge_6$-type structure, means that the asymmetry parameter (η) is zero and V_{zz} lies along a crystallographic axis. Previous studies of orthorhombic RFe_6Sn_6 compounds, showed V_{zz} to be in the ab-plane [24], however, $TbFe_6Sn_4Ge_2$ adopts the hexagonal $HfFe_6Ge_6$-type structure, where V_{zz} is known to be along c [22]. We will therefore consider both cases.

Comparison of $\Delta(T)$ in Fig. 9 with $q_z(T)$ in Fig. 7 shows that the change in quadrupole splitting tracks the changes in q_z, and both saturate at low temperatures. Averaging the points below 30 K gives Δ in the helimagnetic state (0.347(6) mm/s) while the maximum at 45 K is taken as the value in the antiferromagnetic

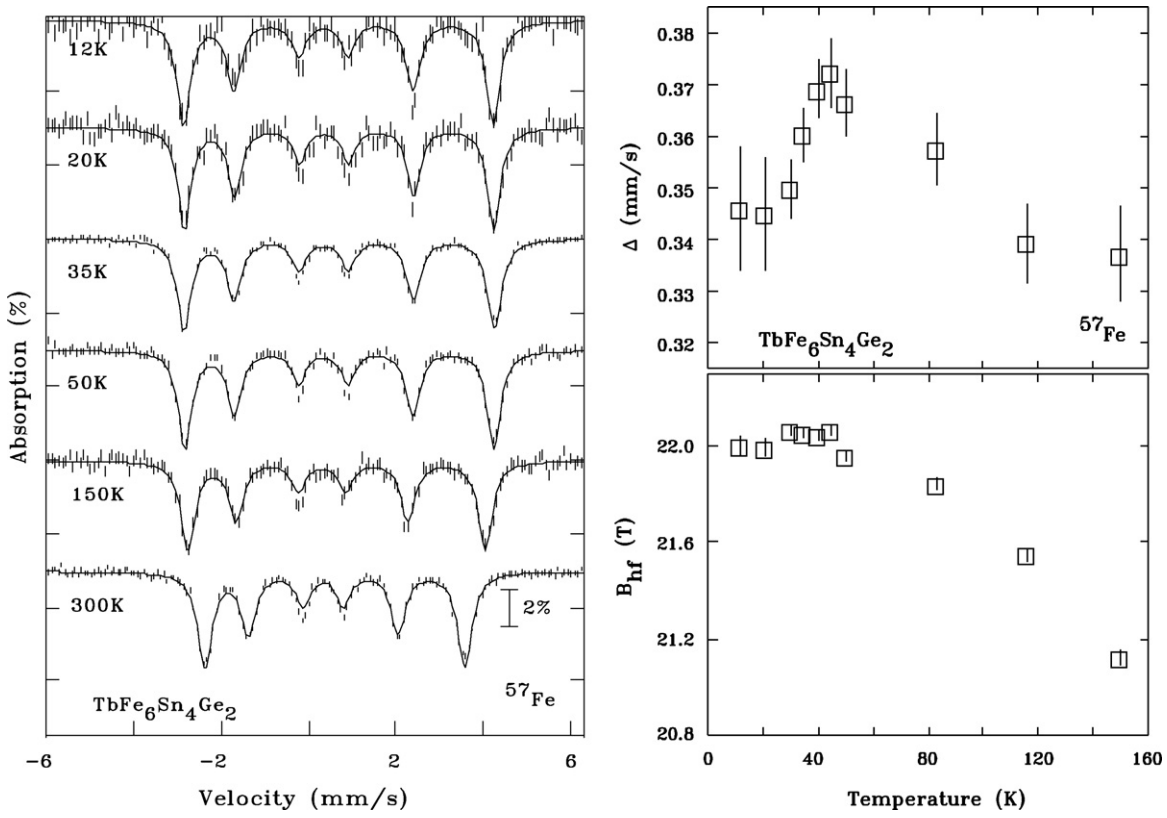

Fig. 9. Left: ^{57}Fe Mössbauer spectra of $TbFe_6Sn_4Ge_2$, from 12 to 300 K. Right: Quadrupole splitting (top) and hyperfine field (bottom) at the Fe site in $TbFe_6Sn_4Ge_2$, obtained through ^{57}Fe Mössbauer spectroscopy.

state. Assuming V_{zz} is parallel to c and using Eq. (2) then yields a canting angle of 12(3)°, consistent with the value of 10(1)° derived from neutron diffraction. If V_{zz} lies in the *ab*-plane, then the helimagnetic ordering of the Fe moments means that θ no longer takes a unique value as the Fe moments turn around the *c*-axis. Averaging over this precession and using the values for Δ derived above, yields the same value for θ, but also predicts a slight increase in linewidth of 0.005 mm/s. This increase is comparable to our linewidth uncertainties and therefore cannot be used to distinguish the two possibilities. Estimating the zero-temperature value of Δ in the antiferromagnetic state by extrapolating the trend from 150 through 45 K yields a slightly larger value of 14(3)° for θ. The canting angle derived from ^{57}Fe Mössbauer spectroscopy is thus independent of the assumed direction of V_{zz} within the crystal axis system, and consistent with that derived from neutron diffraction.

3.3.4. ^{119}Sn Mössbauer spectroscopy

At high temperatures ($T > T_t$), only the Fe sublattice is ordered, and the magnetic structure is layered along *c* as Fe(↑)–Fe(↓)–Tb–Fe(↑)–Fe(↓) (Fig. 3). Sn-2e is very near to one Fe layer, in which all of the moments are parallel. Therefore, Sn-2e sees a large transferred hyperfine field of 20.20(2) T at 50 K, which is parallel to the *c*-axis ($\theta = 0°$). Both Sn-2c and Sn-2d are located between two antiparallel Fe layers, resulting in a zero net transferred hyperfine field at these sites above T_t.

Below $T_t = 42(1)$ K, the Tb sublattice orders helimagnetically in the *ab*-plane, and a helimagnetic contribution arises from the canting of the Fe moments by 12(3)° from *c* (Fig. 8). Although the antiferromagnetic components of the Fe sublattice still cancel around the Sn-2d site, the planar components of the helimagnetic contribution add, generating a small but non-zero transferred B_{hf} at the Sn-2d site that is oriented perpendicular to the c-axis ($\theta = 90°$). This new field is observed for $T \leq 38(3)$ K.

One might also expect a comparable hyperfine field to develop at the Sn-2c site as it has a similar Fe coordination, however none was observed. The continued absence of B_{hf} below T_t at the Sn-2c site may be due to the influence of the three Tb neighbours, although this effect is likely to be small as B_{hf} at the Sn-2e site, which has one Tb neighbour, changes by only ~ 0.1 T on cooling through T_t. The low Sn occupation of the 2c site in this compound greatly limits the detection of a small B_{hf} and it was found that fitting with a single line ($B_{hf} = 0$ T) continued to provide an adequate description of the Sn-2c subspectrum below T_t.

4. Conclusions

The Fe sublattice in $TbFe_6Sn_4Ge_2$ orders antiferromagnetically at 518(3) K, with the Fe moments along the *c*-axis. Below $T_t = 42(1)$ K, the Tb sublattice orders helimagnetically, and imposes helimagnetic order throughout the Fe sublattice, with a canting angle of 10(1)° (neutron diffraction) 12(3)° (^{57}Fe Mössbauer). At 2 K, the Tb moment is $\mu_{Tb} = 6.84(9)\mu_B$, and the Fe moments are $\mu_{Fe}(AF) = 2.34(5)\mu_B$ and $\mu_{Fe}(Heli) = 0.40(4)\mu_B$. Helimagnetic ordering of the Fe sublattice is seen

through analysis of the low temperature neutron diffraction patterns and confirmed by changes in both the ^{57}Fe and the ^{119}Sn Mössbauer spectra.

This study provides the first evidence for coupling between the two sublattices in the RFe_6Sn_6 family. It will be interesting to check whether this behaviour occurs in the other isotypic members (R = Gd–Er) whose crystal structure and bulk magnetic properties have been described [7], or if it is limited to the R=Tb compound. A neutron diffraction and Mössbauer study of the Dy, Ho and Er representatives is currently underway.

References

[1] J.M. Cadogan, D.H. Ryan, J. Alloys Compd. 326 (2001) 166.
[2] G. Venturini, R. Welter, B. Malaman, J. Alloys Compd. 185 (1992) 99.
[3] J.M. Cadogan, D.H. Suharyana, O. Ryan, W. Moze, Kockelmann, IEEE Trans. Magnet. 37 (4) (20012006).
[4] D.H. Ryan, J.M. Cadogan, J. Appl. Phys. 79 (1996) 6004.
[5] X.L. Rao, J.M.D. Coey, J. Appl. Phys. 81 (1997) 5181.
[6] H. Ihou-Mouko, G. Venturini, J. Alloys Compd. 396 (2005) 59.
[7] G. Venturini, J. Alloys Compd. 400 (2005) 37.
[8] J. Rodríguez-Carvajal, Physica B 192 (1993) 55.
[9] C.J. Voyer, MSc. Thesis, McGill University (2005).
[10] B. Chafik El Idrissi, G. Venturini, B. Malaman, Mater. Res. Bull. 26 (12) (1991) 1331.
[11] T. Mazet, B. Malaman, J. Magn. Magn. Mater. 219 (2000) 33.
[12] T. Mazet, O. Isnard, B. Malaman, Sol. State Commun. 114 (2000) 91.
[13] J.M. Cadogan, Suharyana, D.H. Ryan, O. Moze, W. Kockelmann, J. Appl. Phys. 87 (9) (2000) 6046.
[14] J.M. Cadogan, D.H. Ryan, I.P. Swainson, O. Moze, J. Phys.: Condens. Matter. 10 (24) (1998) 5383.
[15] O. Zaharko, P. Schobinger-Papamantellos, C. Ritter, J. Rodriguez-Carvajal, K.H.J. Buschow, J. Magn. Magn. Mater. 187 (1998) 293.
[16] J.M. Cadogan, D.H. Ryan, I.P. Swainson, J. Phys.: Condens. Matter. 12 (2000) 8963.
[17] O. Zaharko, P. Schobinger-Papamantellos, J. Rodríguez-Carvajal, K.H.J. Buschow, J. Alloys Compd. 288 (1–2) (1999) 50.
[18] J.M. Cadogan, D.H. Ryan, O. Moze, M. Suharyana, Hoffman, J. Phys.: Condens. Matter. 15 (10) (2003) 1757.
[19] T. Mazet, B. Malaman, J. Phys.: Condens. Matter. 12 (6) (2000) 1085.
[20] P. Schobinger-Papamantellos, K.H.J. Buschow, F.R. de Boer, C. Ritter, O. Isnard, F. Fauth, J. Alloys Compd. 267 (1–2) (1998) 59.
[21] Laura K. Perry, D.H. Ryan, G. Venturini, J.M. Cadogan, J. Appl. Phys. 99 (8) (2006) 08J302.
[22] Laura K. Perry, D.H. Ryan, G. Venturini, Unpublished.
[23] G. Venturini, B. Chafik El Idrissi, B. Malaman, J. Magn. Magn. Mater. 94 (1991) 35.
[24] Y.B. Wang, J.M. Cadogan, D. Wiarda, D.H. Ryan, IEEE Trans. Magnet. 30 (6) (1994) 4951.